Table 1 Patient demographics[a]

Diagnosis	No. of patients	Mean age (SD), years	Mean PMI (hours)
AD	3	72.9 ± 6.7	22.8 ± 8.8
PSP	3	73.2 ± 4.6	37.2 ± 18.6
PiD	2	75.4 ± 7.1	47.0 ± 5.2
CBD	1	72.5	11.0
PD	1	70.5	22.5

[a]AD, Alzheimer's disease; CBD, Corticobasal degeneration; PD, Parkinson's disease; PiD, Pick's disease; PMI, Postmortem interval; PSP, Progressive supranuclear palsy.

with PSP who underwent PET was 79 years old and had 11 years of formal education. A neuropsychological examination revealed the patient had a Mini Mental State Examination score of 26, a Clinical Dementia Rating Scale score of 1 a Clinical Dementia Rating Scale–Sum of Boxes score of 5.5, an episodic memory composite score of −3.22 and a nonmemory composite score of −3.40. The PSP participant died 5 months after the PET scans were taken.

Assessment of THK523 binding/fluorescence in non–Alzheimer's disease tauopathies

The results of our previous postmortem studies [29] have indicated that THK523 labels AD tau lesions, namely, NFTs in the hippocampus of patients with AD (Figure 1). To determine whether THK523 would also bind to non-AD tau lesions, brain sections from non-AD tauopathies were evaluated. For these studies, fixed contiguous serial sections from the striatum (CBD and PSP samples), the frontal cortex (PiD sample) and the pons (PSP sample) were either immunostained with a polyclonal tau antibody for the detection of tau lesions or incubated with the fluorescent compound THK523 to determine whether THK523 bound to non-AD tauopathy aggregates. Immunohistochemical staining of brain tissue regions rich in tau immunoreactivity was detected by light microscopy, and the same tissue region within the adjacent serial section was assessed by fluorescence microscopy to compare and determine whether the immunoreactive tau lesion colocalised with THK523 binding, indicated by a fluorescent signal. Immunohistological assessment of brain sections from CBD and PiD patients revealed the characteristic presence of globose tangles, coiled bodies (as indicated by the arrowheads in the figures; see top left panel of Figure 2) and Pick's bodies (arrowheads in bottom left panel of Figure 2) in the striatum and frontal cortex. Nonetheless, examination of the same region within the adjacent serial section exhibited no signs of THK523 fluorescence, indicating that THK523 does not bind to these tau lesions. Likewise, immunohistological evaluation of the pons (left, top panel of Figure 3) and striatum (left, bottom panel of Figure 2) in PSP patients revealed that, despite the presence of tau globose tangles, there was no detectable THK523 fluorescence signal in the same region of the adjacent serial brain section, again suggesting that THK523 does not bind to globose tangles. It is noteworthy that one of the three PSP patients evaluated (Figure 3) had had ^{18}F-THK523 and ^{18}F-florbetaben PET scans 5 months prior to death. There was low ^{18}F-florbetaben cortical retention (Figure 4), correlating with postmortem results showing absence of Aβ deposits. There was also low cortical ^{18}F-THK523 retention as well as low ^{18}F-THK523 retention in the basal ganglia, midbrain, pons and cerebellar white matter (Figure 4), which was indistinguishable from age-matched controls and in contrast to the relatively high density of tau lesions observed in the

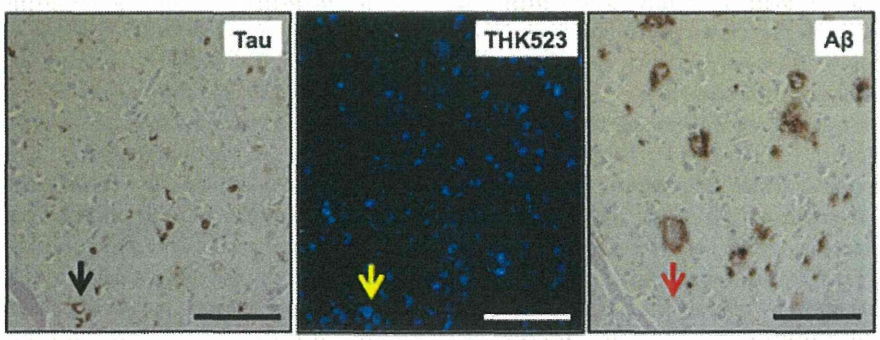

Figure 1 THK523 binds to neurofibrillary tangles in an Alzheimer's disease patient. Microscopy of 5-μm serial sections from the hippocampus of a representative Alzheimer's disease patient. The left image (tau) is the first of three serial sections. It is immunostained with tau polyclonal antibody to detect tau lesions in the hippocampus. The black arrow indicates the positioning of neurofibrillary tangles (NFTs). The positioning of the NFTs indicated by the black arrow was transferred to subsequent adjacent serial sections that were either stained with THK523 (middle image, THK523) or immunostained with a monoclonal antibody raised to amyloid-β (Aβ) to identify senile plaques in the tissue section (right image, Aβ). Fluorescence staining of THK523 (middle) appears to colocalise and resemble tau NFTs, indicated by the yellow arrow, in the absence of Aβ immunoreactivity in the same tissue region (right, red arrow). Tissue section images were obtained using a Zeiss microscope and an AxioCam digital camera (Carl Zeiss Microscopy, North Ryde, Australia). Scale bars, 100 μm.

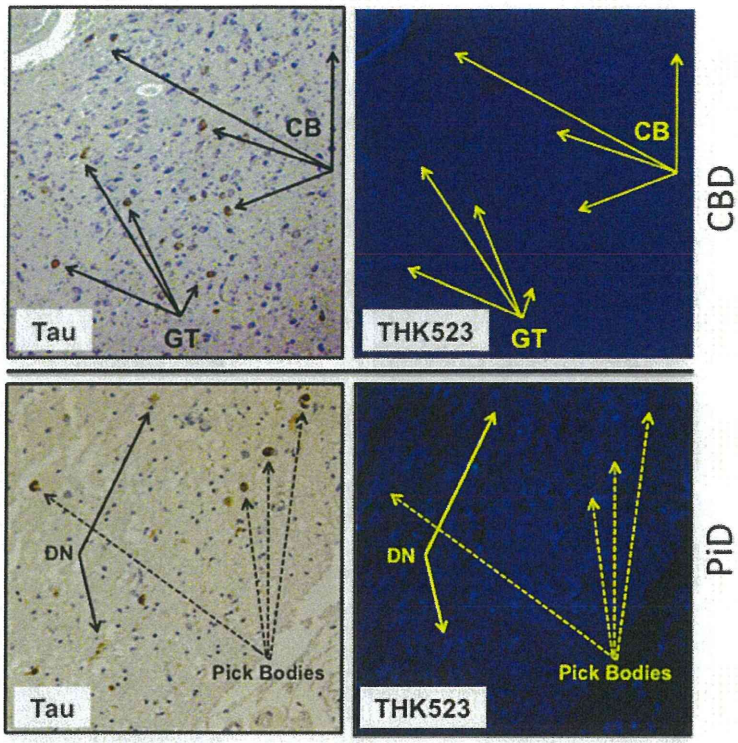

Figure 2 THK523 does not bind to tau lesions in corticobasal degeneration or Pick's disease. Microscopy of 5-μm serial sections from the striatum of a corticobasal degeneration (CBD) patient (top panel) and the frontal cortex of a Pick's disease (PiD) patient (bottom panel). The left side (Tau) shows the first of two serial sections immunostained with tau polyclonal antibodies to detect tau lesions. The arrows indicate the positioning of brown immunostained globose tangles (GT) and coiled bodies (CB; top panel) in a CBD patient and Pick's bodies and dystrophic neurites (DN) (bottom panel). The same region of tissue was subsequently imaged for the adjacent section, which was stained with THK523 (right, THK523). The positioning of the tau lesion arrows was transferred to the adjacent stained serial section and is indicated by yellow arrows (THK523). The absence of fluorescence suggests that THK523 does not bind to CBD or PiD tau lesions. Tissue sections were imaged using a Zeiss microscope and an AxioCam digital camera at 5× (CBD) and 20× (PiD) original magnification.

brain, confirming the absence of THK523 binding to globose tangles. Analysis of the PSP patient PET scans showed global and regional Z-scores less than 1.0 for ^{18}F-THK523 and ^{18}F-florbetaben, confirming the visual inspection of the images.

Assessment of THK523 binding/fluorescence in Parkinson's disease

To further test the selectivity of THK523, we evaluated its ability to bind to Lewy bodies composed of α-synuclein and ubiquitin aggregates sharing a similar β-sheet secondary structure. For these studies, serial sections of the substantia nigra from a PD patient were either immunostained with antibodies raised to α-synuclein, or treated with a fluorescent compound, THK523. Evaluation of these stained serial sections demonstrated that, whilst the presence of Lewy bodies could be clearly identified by immunohistochemistry (Figure 5, left panel), the adjacent serial section was devoid of THK523 fluorescence (Figure 5, right panel), implying that THK523 did not bind to Lewy bodies.

Discussion

In the present study, we further characterized ^{18}F-THK523 as a selective tau imaging agent by testing its ability to recognize the various morphological conformations of tau in a wide spectrum of tauopathies. Whilst in our previous studies we determined that THK523 binds selectively to NFTs in preference to Aβ plaques [29,32], in this study we also assessed ^{18}F-THK523 binding to other β-sheet structured protein fibrils, namely, α-synuclein-containing Lewy bodies.

Given the morphological and ultrastructural diversity of tau aggregates, it may be unlikely that a single tau imaging agent could be useful for the diagnosis of all tauopathies. In the first instance, tau comprises six isoforms distinguished by their length and number of repeats (R) of microtubule binding domains [6,42]. AD tau comprises an equal ratio of the 3R and 4R isoforms, which mainly appear as NFTs. The 4R isoform predominates in PSP with tau aggregates comprising tufted-shaped astrocytes, GTs and oligodendroglial coiled bodies [43,44]. Despite also being a 4R tauopathy, in CBD the tau inclusions

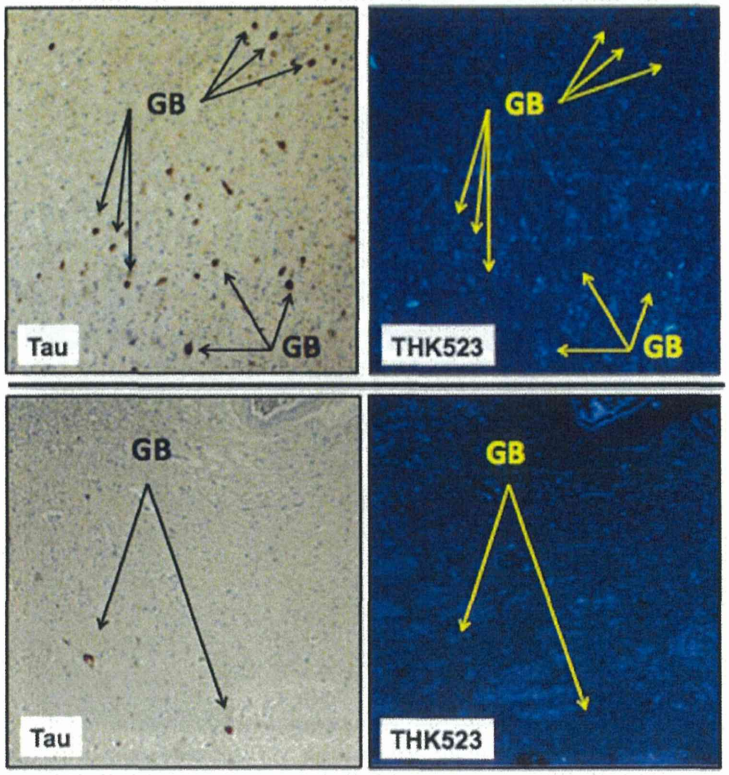

Figure 3 THK523 does not bind to globose tangles in a progressive supranuclear palsy patient. Microscopy of 5-μm serial sections taken from the pons (top panels) and the striatum (bottom panels) of a representative progressive supranuclear palsy (PSP) patient. Left (Tau) images show the first of two serial sections immunostained with a tau polyclonal antibody to detect globose tangles (GB). The black arrows indicate the positioning of brown immunostained GBs in the tissue section examined. The same region of tissue was subsequently imaged for the adjacent section, which was treated with THK523 (right, THK523). The positioning of the tau lesion black arrows was transferred to the adjacent stained serial section and is indicated by the yellow arrows (THK523). The absence of fluorescence suggests that THK523 did not bind to the tau lesions of the PSP patients examined. Tissue sections were imaged using a Zeiss microscope and an AxioCam digital camera at 5× original magnification.

appear as astrocytic plaques, neutropil threads and tau pretangles [45]. PiD, a 3R tauopathy, is diagnosed by the presence of 'Pick bodies', tau-positive intraneuronal inclusions [46]. Moreover, these tau aggregates are further differentiated by their ultrastructure. NFTs are predominantly composed of paired helical filaments (PHFs), tau inclusions in PSP and CBD are composed predominantly of straight tau filaments (SFs) and twisted tau filaments (TFs) [11], whereas Pick bodies comprise a combination of TFs and random coiled tau filaments [11]. It is noteworthy that, whilst PSP and CBD share SFs, the size of the filaments is significantly different [47]. Despite this diversity, a recent report describing a novel class of tau tracers phenyl/pyridinyl-butadienyl-benzothiazoles/benzothiazoliums (PBB) demonstrated binding to a variety of tau deposits in fluorescence studies of AD, CBD and PSP brain sections [48]. Additionally, that study also demonstrated positive [^{11}C]PBB3 PET scans in both AD and CBD patients [48].

Given the evident differences in THK523 staining, the fluorescence microscopy studies we present herein demonstrate that THK523, even at the very high concentration of 100 μM, does not bind to non-PHF-tau aggregates. The existence of a THK523 binding site on PHFs that is absent in the other conformations is further emphasized by previous computerized cross-sectional and fragmentation studies which indicated that, whilst these types of filaments share a similarly shaped morphological unit, the filament arrangement is different [49].

PHFs appear as two filaments twisted around one another with a cross-over repeat of 80 nm and an apparent width varying between about 10 nm and 22 nm [50]. The resulting aggregate exhibits an amyloid structure characterized by a β-sheet network forming the heart of the protofibril network. This ultrastructural property shared with Aβ and α-synuclein aggregates sometimes results in the nonselective binding of imaging agents [51]. As noted previously [29], in addition to THK523's

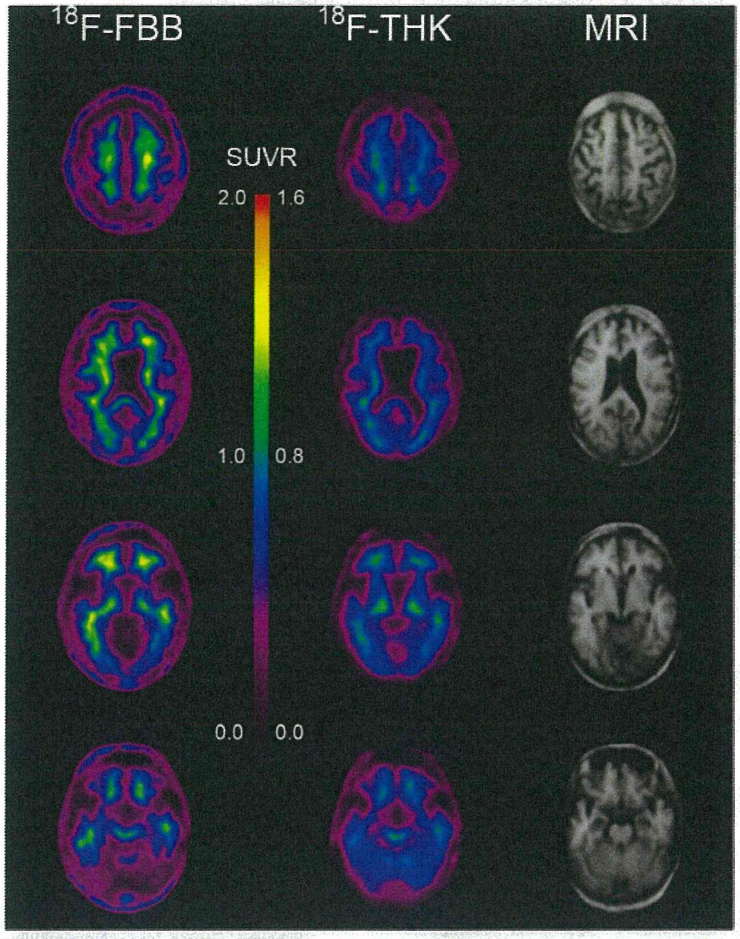

Figure 4 ^{18}F-THK523 and ^{118}F-florbetaben positron emission tomography scans in a progressive supranuclear palsy patient. Representative ^{18}F-florbetaben (^{18}F-FBB, left) and ^{18}F-THK523 (^{18}F-THK, right) transaxial images at three different brain levels of a 79–year-old PSP patient with a Mini Mental State Examination score of 26. Visual inspection reveals no cortical retention of either ^{18}F-THK523 or ^{18}F-florbetaben, despite a postmortem immunohistological examination (see Figure 3 5 months after PET evaluation), confirming the presence of tau lesions. SUVR, Standardised uptake value ratio.

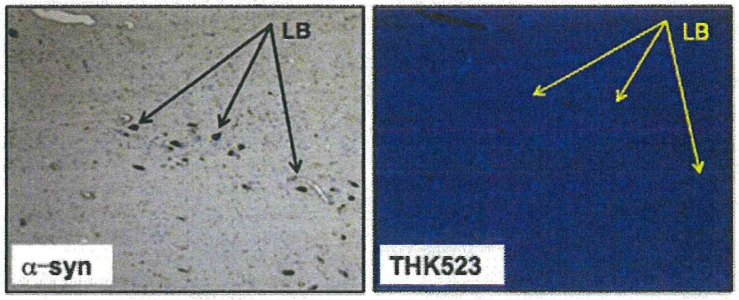

Figure 5 THK523 does not bind to Lewy bodies in Parkinson's disease patient. Microscopy of 5-μm serial sections from the substantia nigra of a Parkinson's disease patient. The left image (α-syn shows the first of two serial sections. It immunostained with an α-synuclein antibody to detect Lewy bodies (LB) in the substantia nigra. The black arrows indicate the positioning of LBs. The same region of tissue was subsequently imaged for the adjacent sections, which were treated with THK523. The positions indicated by the black arrows in the left panel were transferred to the adjacent THK523 serial section and are indicated by the yellow arrows (THK523). The absence of fluorescence staining indicates that THK523 does not bind to α-synuclein containing Lewy bodies in the same tissue region. Tissue sections were imaged using a Zeiss microscope and an AxioCam digital camera at 5× original magnification.

binding to NFTs, our fluorescence studies obtained at high tracer concentrations—10,000-fold higher than the concentrations typically achieved during a PET scan—demonstrated inconsistent THK523 staining of Aβ plaques. THK523 stained the dense core of some Aβ plaques in the frontal cortex of AD sections but did not stain dense Aβ plaques in the hippocampus (Figure 1, right panel). It is noteworthy that variable staining of NFTs at high concentrations of PiB has also been reported [52]. In addition to previous reports of *in vitro* studies [29,30], several lines of evidence support the notion that THK523 selectively binds to PHF-tau and does not bind to Aβ *in vivo*: (1) Cortical THK523 retention is significantly higher in AD; (2) THK523 retention follows the known distribution of PHF-tau in the AD brain; (3) PiB and THK523 show different brain regional distribution patterns; (4) hippocampal THK523 retention significantly correlated with cognitive parameters, but hippocampal PiB retention did not; and (5) hippocampal THK523 retention significantly correlated with hippocampal volume, but hippocampal PiB retention did not [32].

The selectivity of THK523 for tau over other β-sheet aggregated proteins was further demonstrated by fluorescence microscopy studies showing the absence of THK523 fluorescence in brain sections exhibiting immunolabelled α-synuclein-containing Lewy bodies (Figure 5, right panel).

The PSP patient showed neither ^{18}F-THK523 nor ^{18}F-florbetaben retention in the brain, suggesting the absence not only of Aβ plaques but also of tau deposits. Neuropathological examination of the brain confirmed the absence of Aβ plaques; however, typical tau lesions were present in different brain regions that were not stained by THK523. Given the ultrastructural diversity of tau aggregates, the information derived from these THK523 studies is highly valuable for the future design of tau imaging ligands.

Conclusion

In the present study, we have demonstrated that THK523 selectively binds to PHF-tau with negligible binding to PSP, CBD and PiD tau aggregates, as well as to Aβ and α-synuclein aggregates. The results of this study also show that novel tracers that bind to non-PHF tau aggregates are needed.

Abbreviations

AD: Alzheimer's disease; Aβ: Amyloid-β; CBD: Corticobasal degeneration; CDR: Clinical Dementia Rating Scale; CDR-SOB: Clinical Dementia Rating Scale–Sum of Boxes; CSF: Cerebrospinal fluid; FTLD: Frontotemporal lobar degeneration; GM: Grey matter; MMSE: Mini Mental State Examination; NFT: Neurofibrillary tangle; PET: Positron emission tomography; PiB: Pittsburgh compound B; PiD: Pick's disease; PSP: Progressive supranuclear palsy; ROI: Region of interest; SF: Straight filament; SUV: Standardised uptake value; TF: Twisted filament.

Competing interests

The authors declare that they have no competing interests.

Authors' contributions

VLV, MTF-T, KY, NO and CLM designed the experiments. SF, RSM, RH, KY, YK and NO designed and manufactured THK523. LT and IB planned and conducted the human brain section immunostaining experiments. CAM planned and conducted the pathological characterisation of human brain samples. VL and CCR planned and coordinated human PET studies. MTF-T and VLV drafted the manuscript. All authors read and approved the final manuscript.

Acknowledgements

We thank Fairlie Hinton and Geoff Pavey from the Victorian Brain Bank Network (VBBN) for sourcing and preparing the human brain tissue (HREC University of Melbourne 9414748). The VBBN is supported by The Florey Institute of Neuroscience and Mental Health, The Alfred and the Victorian Forensic Institute of Medicine, and it is funded by Australia's National Health & Medical Research Council (NHMRC) and Parkinson's Victoria. The research was supported in part by Alzheimer's Drug Discovery Foundation Research Grant 20101208 AFTD and NHMRC project grant 1044361.

Author details

[1]The Florey Institute of Neuroscience and Mental Health, 30 Royal Parade, Parkville, 3052 Melbourne, Victoria, Australia. [2]Department of Nuclear Medicine & Centre for PET, Austin Health, 145 Studley Road, Heidelberg, 3084 Melbourne, Victoria, Australia. [3]Department Pharmacology, Tohoku University School of Medicine, Sendai, Japan. [4]Department of Anatomical Pathology, The Alfred Hospital, Monash University, Melbourne, Australia. [5]Innovation of New Biomedical Engineering Center, Tohoku University, Sendai, Japan.

Received: 11 July 2013 Accepted: 13 February 2014
Published: 26 February 2014

References

1. Masters CL, Cappai R, Barnham KJ, Villemagne VL: **Molecular mechanisms for Alzheimer's disease: implications for neuroimaging and therapeutics.** *J Neurochem* 2006, **97**:1700–1725.
2. van der Zee J, Sleegers K, Van Broeckhoven C: **Invited article: the Alzheimer disease–frontotemporal lobar degeneration spectrum.** *Neurology* 2008, **71**:1191–1197.
3. Braak H, Braak E: **Morphological criteria for the recognition of Alzheimer's disease and the distribution pattern of cortical changes related to this disorder.** *Neurobiol Aging* 1994, **15**:355–356. discussion 379–380.
4. Corder EH, Woodbury MA, Volkmann I, Madsen DK, Bogdanovic N, Winblad B: **Density profiles of Alzheimer disease regional brain pathology for the Huddinge Brain Bank: pattern recognition emulates and expands upon Braak staging.** *Exp Gerontol* 2000, **35**:851–864.
5. The National Institute on Aging and Reagan Institute Working Group on Diagnostic Criteria for the Neuropathological Assessment of Alzheimer's Disease: **Consensus recommendations for the postmortem diagnosis of Alzheimer's disease.** *Neurobiol Aging* 1997, **18**:S1–S2.
6. Delacourte A: **Tauopathies: recent insights into old diseases.** *Folia Neuropathol* 2005, **43**:244–257.
7. King ME, Ghoshal N, Wall JS, Binder LI, Ksiezak-Reding H: **Structural analysis of Pick's disease-derived and *in vitro*-assembled tau filaments.** *Am J Pathol* 2001, **158**:1481–1490.
8. Scaravilli T, Tolosa E, Ferrer I: **Progressive supranuclear palsy and corticobasal degeneration: lumping versus splitting.** *Mov Disord* 2005, **20**:S21–S28.
9. Uchihara T, Tsuchiya K: **Neuropathology of Pick body disease.** *Handb Clin Neurol* 2008, **89**:415–430.
10. Mohorko N, Bresjanac M: **[Tau protein and human tauopathies: an overview] [in Slovenian].** *Zdrav Vestn* 2008, **77**:II-35–II-41.
11. Delacourte A, Buée L: **Tau pathology: a marker of neurodegenerative disorders.** *Curr Opin Neurol* 2000, **13**:371–376.
12. Villemagne VL, Furumoto S, Fodero-Tavoletti M, Harada R, Mulligan RS, Kudo Y, Masters CL, Yanai K, Rowe CC, Okamura N: **The challenges of tau imaging.** *Future Neurol* 2012, **7**:409–421.
13. Dickson DW: **Neuropathology of Pick's disease.** *Neurology* 2001, **56**:S16–S20.

14. Josephs KA, Whitwell JL, Dickson DW, Boeve BF, Knopman DS, Petersen RC, Parisi JE, Jack CR Jr: **Voxel-based morphometry in autopsy proven PSP and CBD.** *Neurobiol Aging* 2008, **29**:280–289.
15. Dickson DW: **Neuropathologic differentiation of progressive supranuclear palsy and corticobasal degeneration.** *J Neurol* 1999, **246**:II6–II15.
16. Cairns NJ, Bigio EH, Mackenzie IRA, Neumann M, Lee VM, Hatanpaa KJ, White CL 3rd, Schneider JA, Grinberg LT, Halliday G, Duyckaerts C, Lowe JS, Holm IE, Tolnay M, Okamoto K, Yokoo H, Murayama S, Woulfe J, Munoz DG, Dickson DW, Ince PG, Trojanowski JQ, Mann DM, Consortium for Frontotemporal Lobar Degeneration: **Neuropathologic diagnostic and nosologic criteria for frontotemporal lobar degeneration: consensus of the Consortium for Frontotemporal Lobar Degeneration.** *Acta Neuropathol* 2007, **114**:5–22.
17. Boxer AL, Geschwind MD, Belfor N, Gorno-Tempini ML, Schauer GF, Miller BL, Weiner MW, Rosen HJ: **Patterns of brain atrophy that differentiate corticobasal degeneration syndrome from progressive supranuclear palsy.** *Arch Neurol* 2006, **63**:81–86.
18. Jack CR Jr, Knopman DS, Jagust WJ, Shaw LM, Aisen PS, Weiner MW, Petersen RC, Trojanowski JQ: **Hypothetical model of dynamic biomarkers of the Alzheimer's pathological cascade.** *Lancet Neurol* 2010, **9**:119–128.
19. Gozes I, Stewart A, Morimoto B, Fox A, Sutherland K, Schmeche D: **Addressing Alzheimer's disease tangles: from NAP to AL-108.** *Curr Alzheimer Res* 2009, **6**:455–460.
20. Hampel H, Blennow K, Shaw LM, Hoessler YC, Zetterberg H, Trojanowski JQ: **Total and phosphorylated tau protein as biological markers of Alzheimer's disease.** *Exp Gerontol* 2010, **45**:30–40.
21. Wada T, Miyata T, Sakai H, Kurokawa K: **β2-microglobulin and renal bone disease.** *Perit Dial Int* 1999, **19**:S413–S416.
22. Wider C, Uitti RJ, Wszolek ZK, Fang JY, Josephs KA, Baker MC, Rademakers R, Hutton ML, Dickson DW: **Progranulin gene mutation with an unusual clinical and neuropathologic presentation.** *Mov Disord* 2008, **23**:1168–1173.
23. Wischik C, Staff R: **Challenges in the conduct of disease-modifying trials in AD: practical experience from a phase 2 trial of Tau-aggregation inhibitor therapy.** *J Nutr Health Aging* 2009, **13**:367–369.
24. Cui M: **Past and recent progress of molecular imaging probes for β-amyloid plaques in the brain.** *Curr Med Chem* 2014, **21**:82–112.
25. Klunk WE, Engler H, Nordberg A, Wang Y, Blomqvist G, Holt DP, Bergström M, Savitcheva I, Huang GF, Estrada S, Ausén B, Debnath ML, Barletta J, Price JC, Sandell J, Lopresti BJ, Wall A, Koivisto P, Antoni G, Mathis CA, Långström B: **Imaging brain amyloid in Alzheimer's disease with Pittsburgh Compound-B.** *Ann Neurol* 2004, **55**:306–319.
26. Rowe CC, Ng S, Ackermann U, Gong SJ, Pike K, Savage G, Cowie TF, Dickinson KL, Maruff P, Darby D, Smith C, Woodward M, Merory J, Tochon-Danguy H, O'Keefe G, Klunk WE, Mathis CA, Price JC, Masters CL, Villemagne VL: **Imaging β-amyloid burden in aging and dementia.** *Neurology* 2007, **68**:1718–1725.
27. Clark CM, Schneider JA, Bedell BJ, Beach TG, Bilker WB, Mintun MA, Pontecorvo MJ, Hefti F, Carpenter AP, Flitter ML, Krautkramer MJ, Kung HF, Coleman RE, Doraiswamy PM, Fleisher AS, Sabbagh MN, Sadowsky CH, Reiman EP, Zehntner SP, Skovronsky DM, AV45-A07 Study Group: **Use of florbetapir-PET for imaging β-amyloid pathology.** *JAMA* 2011, **305**:275–283.
28. Vandenberghe R, Van Laere K, Ivanoiu A, Salmon E, Bastin C, Triau E, Hasselbalch S, Law I, Andersen A, Korner A, Minthon L, Garraux G, Nelissen N, Bormans G, Buckley C, Owenius R, Thurfjell L, Farrar G, Brooks DJ: **^{18}F-flutemetamol amyloid imaging in Alzheimer disease and mild cognitive impairment: a phase 2 trial.** *Ann Neurol* 2010, **68**:319–329.
29. Fodero-Tavoletti MT, Okamura N, Furumoto S, Mulligan RS, Connor AR, McLean CA, Cao D, Rigopoulos A, Cartwright GA, O'Keefe G, Gong S, Adlard PA, Barnham KJ, Rowe CC, Masters CL, Kudo Y, Cappai R, Yanai K, Villemagne VL: **^{18}F-THK523: a novel *in vivo* tau imaging ligand for Alzheimer's disease.** *Brain* 2011, **134**:1089–1100.
30. Harada R, Okamura N, Furumoto S, Tago T, Maruyama M, Higuchi M, Yoshikawa T, Arai H, Iwata R, Kudo Y, Yanai K: **Comparison of the binding characteristics of [^{18}F]THK-523 and other amyloid imaging tracers to Alzheimer's disease pathology.** *Eur J Nucl Med Mol Imaging* 2013, **40**:125–132.
31. Okamura N, Suemoto T, Furumoto S, Suzuki M, Shimadzu H, Akatsu H, Yamamoto T, Fujiwara H, Nemoto M, Maruyama M, Arai H, Yanai K, Sawada T, Kudo Y: **Quinoline and benzimidazole derivatives: candidate probes for *in vivo* imaging of tau pathology in Alzheimer's disease.** *J Neurosci* 2005, **25**:10857–10862.
32. Villemagne VL, Furumoto S, Fodero-Tavoletti MT, Mulligan RS, Hodges J, Harada R, Yates P, Piguet O, Pejoska S, Doré V, Yanai K, Masters CL, Kudo Y, Rowe CC, Okamura N: ***In vivo* evaluation of a novel tau imaging tracer for Alzheimer's disease.** *Eur J Nucl Med Mol Imaging* 2014. [Epub ahead of print]. doi:10.1007/s00259-013-2681-7.
33. Hauw JJ, Daniel SE, Dickson D, Horoupian DS, Jellinger K, Lantos PL, McKee A, Tabaton M, Litvan I: **Preliminary NINDS neuropathologic criteria for Steele-Richardson-Olszewski syndrome (progressive supranuclear palsy).** *Neurology* 1994, **44**:2015–2019.
34. Lowe J: **Part 7: Frontotemporal Lobar Degeneration and Amyotrophic Lateral Sclerosis/Motor Neuron Disease. Chapter 40: Introduction.** In *Neurodegeneration: The Molecular Pathology of Dementia and Movement Disorders. 2nd edition. Edited by Dickson D, Weller RO. Oxford, UK:* Wiley-Blackwell; 2011:389–390.
35. Culvenor JG, McLean CA, Cutt S, Campbell BC, Maher F, Jäkälä P, Hartmann T, Beyreuther K, Masters CL, Li QX: **Non-Aβ component of Alzheimer's disease amyloid (NAC) revisited: NAC and α-synuclein are not associated with Aβ amyloid.** *Am J Pathol* 1999, **155**:1173–1181.
36. Culvenor JG, Henry A, Hartmann T, Evin G, Galatis D, Friedhuber A, Jayasena UL, Underwood JR, Beyreuther K, Masters CL, Cappai R: **Subcellular localization of the Alzheimer's disease amyloid precursor protein and derived polypeptides expressed in a recombinant yeast system.** *Amyloid* 1998, **5**:79–89.
37. Villemagne V, Fodero-Tavoletti M, Furumoto S, Mulligan RS, Hodges J, Piguet O, Pejoska S, Kudo Y, Masters C, Yanai K, Rowe C, Okamura N: ***In vivo* tau imaging in Alzheimer's disease and other dementias.** *Alzheimers Dement* 2012, **8**:699.
38. Villemagne VL, Fodero-Tavoletti MT, Pike KE, Cappai R, Masters CL, Rowe CC: **The ART of loss: Aβ imaging in the evaluation of Alzheimer's disease and other dementias.** *Mol Neurobiol* 2008, **38**:1–15.
39. Rowe CC, Ackerman U, Browne W, Mulligan R, Pike KL, O'Keefe G, Tochon-Danguy H, Chan G, Berlangieri SU, Jones G, Dickinson-Rowe KL, Kung HP, Zhang W, Kung MP, Skovronsky D, Dyrks T, Holl G, Krause S, Friebe M, Lehman L, Lindemann S, Dinkelborg LM, Masters CL, Villemagne VL: **Imaging of amyloid β in Alzheimer's disease with ^{18}F-BAY94-9172, a novel PET tracer: proof of mechanism.** *Lancet Neurol* 2008, **7**:129–135.
40. Villemagne VL, Pike KE, Chételat G, Ellis KA, Mulligan RS, Bourgeat P, Ackermann U, Jones G, Szoeke C, Salvado O, Martins R, O'Keefe G, Mathis CA, Klunk WE, Ames D, Masters CL, Rowe CC: **Longitudinal assessment of Aβ and cognition in aging and Alzheimer disease.** *Ann Neurol* 2011, **69**:181–192.
41. Good CD, Johnsrude IS, Ashburner J, Henson RN, Friston KJ, Frackowiak RS: **A voxel-based morphometric study of ageing in 465 normal adult human brains.** *Neuroimage* 2001, **14**:21–36.
42. Sergeant N, Bretteville A, Hamdane M, Caillet-Boudin ML, Grognet P, Bombois S, Blum D, Delacourte A, Pasquier F, Vanmechelen E, Schraen-Maschke S, Buée L: **Biochemistry of Tau in Alzheimer's disease and related neurological disorders.** *Expert Rev Proteomics* 2008, **5**:207–224.
43. Williams DR, Holton JL, Strand C, Pittman A, de Silva R, Lees AJ, Revesz T: **Pathological tau burden and distribution distinguishes progressive supranuclear palsy-parkinsonism from Richardson's syndrome.** *Brain* 2007, **130**:1566–1576.
44. Yamada T, McGeer PL, McGeer EG: **Appearance of paired nucleated, Tau-positive glia in patients with progressive supranuclear palsy brain tissue.** *Neurosci Lett* 1992, **135**:99–102.
45. Dickson DW, Bergeron C, Chin SS, Duyckaerts C, Horoupian D, Ikeda K, Jellinger K, Lantos PL, Lippa CF, Mirra SS, Tabaton M, Vonsattel JP, Wakabayashi K, Litvan I, Office of Rare Diseases of the National Institutes of Health: **Office of Rare Diseases neuropathologic criteria for corticobasal degeneration.** *J Neuropathol Exp Neurol* 2002, **61**:935–946.
46. Buée L, Delacourte A: **Comparative biochemistry of tau in progressive supranuclear palsy, corticobasal degeneration, FTDP-17 and Pick's disease.** *Brain Pathol* 1999, **9**:681–693.
47. Arima K: **Ultrastructural characteristics of tau filaments in tauopathies: immuno-electron microscopic demonstration of tau filaments in tauopathies.** *Neuropathology* 2006, **26**:475–483.
48. Maruyama M, Shimada H, Suhara T, Shinotoh H, Ji B, Maeda J, Zhang MR, Trojanowski JQ, Lee VM, Ono M, Masamoto K, Takano H, Sahara N, Iwata N, Okamura N, Furumoto S, Kudo Y, Chang Q, Saido TC, Takashima A, Lewis J,

Jang MK, Aoki I, Ito H, Higuchi M: **Imaging of tau pathology in a tauopathy mouse model and in Alzheimer patients compared to normal controls.** *Neuron* 2013, **79**:1094–1108.
49. Crowther RA: **Straight and paired helical filaments in Alzheimer disease have a common structural unit.** *Proc Natl Acad Sci U S A* 1991, **88**:2288–2292.
50. Bulic B, Pickhardt M, Mandelkow EM, Mandelkow E: **Tau protein and tau aggregation inhibitors.** *Neuropharmacology* 2010, **59**:276–289.
51. Agdeppa ED, Kepe V, Liu J, Flores-Torres S, Satyamurthy N, Petric A, Cole GM, Small GW, Huang SC, Barrio JR: **Binding characteristics of radiofluorinated 6-dialkylamino-2-naphthylethylidene derivatives as positron emission tomography imaging probes for β-amyloid plaques in Alzheimer's disease.** *J Neurosci* 2001, **21**:RC189.
52. Ikonomovic MD, Klunk WE, Abrahamson EE, Mathis CA, Price JC, Tsopelas ND, Lopresti BJ, Ziolko S, Bi W, Paljug WR, Debnath ML, Hope CE, Isanski BA, Hamilton RL, DeKosky ST: **Post-mortem correlates of *in vivo* PiB-PET amyloid imaging in a typical case of Alzheimer's disease.** *Brain* 2008, **131**:1630–1645.

doi:10.1186/alzrt240
Cite this article as: Fodero-Tavoletti *et al.*: Assessing THK523 selectivity for tau deposits in Alzheimer's disease and non–Alzheimer's disease tauopathies. *Alzheimer's Research & Therapy* 2014 **6**:11.

doi:10.1093/brain/awu064 Brain 2014: 137; 1762–1771 | 1762

BRAIN
A JOURNAL OF NEUROLOGY

Non-invasive assessment of Alzheimer's disease neurofibrillary pathology using ^{18}F-THK5105 PET

Nobuyuki Okamura,[1] Shozo Furumoto,[2] Michelle T. Fodero-Tavoletti,[3,4] Rachel S. Mulligan,[4] Ryuichi Harada,[1] Paul Yates,[4] Svetlana Pejoska,[4] Yukitsuka Kudo,[5] Colin L. Masters,[3,6] Kazuhiko Yanai,[1,2] Christopher C. Rowe[4] and Victor L. Villemagne[3,4]

1 Department of Pharmacology, Tohoku University School of Medicine, Sendai, Japan
2 Cyclotron and Radioisotope Centre, Tohoku University, Sendai, Japan
3 The Florey Institute of Neuroscience and Mental Health, The University of Melbourne, Australia
4 Centre for PET, Austin Health, Melbourne, Australia
5 Clinical Research, Innovation and Education Centre, Tohoku University Hospital, Sendai, Japan
6 The Mental Health Research Institute, Melbourne, Australia

Correspondence to: Nobuyuki Okamura,
Department of Pharmacology,
Tohoku University School of Medicine,
2-1 Seiryo-machi, Aoba-ku,
Sendai, 9808575, Japan
E-mail: nookamura@med.tohoku.ac.jp

Non-invasive imaging of tau pathology in the living brain would be useful for accurately diagnosing Alzheimer's disease, tracking disease progression, and evaluating the treatment efficacy of disease-specific therapeutics. In this study, we evaluated the clinical usefulness of a novel tau-imaging positron emission tomography tracer ^{18}F-THK5105 in 16 human subjects including eight patients with Alzheimer's disease (three male and five females, 66–82 years) and eight healthy elderly controls (three male and five females, 63–76 years). All participants underwent neuropsychological examination and 3D magnetic resonance imaging, as well as both ^{18}F-THK5105 and ^{11}C-Pittsburgh compound B positron emission tomography scans. Standard uptake value ratios at 90–100 min and 40–70 min post-injection were calculated for ^{18}F-THK5105 and ^{11}C-Pittsburgh compound B, respectively, using the cerebellar cortex as the reference region. As a result, significantly higher ^{18}F-THK5105 retention was observed in the temporal, parietal, posterior cingulate, frontal and mesial temporal cortices of patients with Alzheimer's disease compared with healthy control subjects. In patients with Alzheimer's disease, the inferior temporal cortex, which is an area known to contain high densities of neurofibrillary tangles in the Alzheimer's disease brain, showed prominent ^{18}F-THK5105 retention. Compared with high frequency (100%) of ^{18}F-THK5105 retention in the temporal cortex of patients with Alzheimer's disease, frontal ^{18}F-THK5105 retention was less frequent (37.5%) and was only observed in cases with moderate-to-severe Alzheimer's disease. In contrast, ^{11}C-Pittsburgh compound B retention was highest in the posterior cingulate cortex, followed by the ventrolateral prefrontal, anterior cingulate, and superior temporal cortices, and did not correlate with ^{18}F-THK5105 retention in the neocortex. In healthy control subjects, ^{18}F-THK5105 retention was ~10% higher in the mesial temporal cortex than in the neocortex. Notably, unlike ^{11}C-Pittsburgh compound B, ^{18}F-THK5105 retention was significantly correlated with cognitive parameters, hippocampal and whole brain grey matter volumes, which was consistent with findings from previous post-mortem studies showing significant correlations of neurofibrillary tangle density with dementia severity or neuronal loss. From these results, ^{18}F-THK5105 positron emission tomography is considered to be useful for the non-invasive assessment of tau pathology in the living brain. This technique would be applicable to the longitudinal evaluation of tau deposition and allow a better understanding of the pathophysiology of Alzheimer's disease.

Received December 11, 2013. Revised January 12, 2014. Accepted February 4, 2014. Advance Access publication March 27, 2014

Keywords: Alzheimer's disease; Alzheimer's disease pathology; amyloid; positron emission tomography; PET

Abbreviations: CDR = clinical dementia rating; MMSE = Mini-Mental State Examination; PiB = Pittsburgh compound B; SOB = sum of boxes; SUV = standardized uptake value; SUVR = ratio of regional SUV to cerebellar cortex SUV ratio

Introduction

Senile plaques and neurofibrillary tangles are considered the major pathological hallmarks of Alzheimer's disease (Braak and Braak, 1991). Senile plaques consist of extracellular aggregates of amyloid-β peptide cleaved from a longer amyloid precursor protein (Masters *et al.*, 2006). The neocortical deposition of senile plaques is considered one of the earliest pathological alterations in Alzheimer's disease and is observed even in the presymptomatic stages (Mintun *et al.*, 2006; Rowe *et al.*, 2007; Price *et al.*, 2009). Recently proposed research diagnostic criteria for preclinical Alzheimer's disease include cognitively intact elderly with abnormal amyloid-β deposition in the brain (Sperling *et al.*, 2011). Preclinical Alzheimer's disease is associated with future cognitive decline and mortality (Vos *et al.*, 2013); however, several neuropathological studies have shown no significant association between density of amyloid-β plaques and the severity of dementia or neuronal loss (Arriagada *et al.*, 1992; Bierer *et al.*, 1995; Gomez-Isla *et al.*, 1997), suggesting the involvement of other key factors in Alzheimer's disease-related neurodegeneration.

Neurofibrillary tangles are comprised of paired helical filaments that result from the abnormal aggregation of tau protein (Grundke-Iqbal *et al.*, 1986*a*, *b*; Lee *et al.*, 1991). Initial neurofibrillary tangle lesions occur in the trans-entorhinal cortex, followed by entorhinal cortex and hippocampus involvement, progressing to temporal neocortex and finally to the other neocortical areas (Arnold *et al.*, 1991; Braak and Braak, 1991). In contrast with senile plaques, neurofibrillary tangle formation correlates well with cognitive impairment severity (Arriagada *et al.*, 1992; Berg *et al.*, 1993; Bierer *et al.*, 1995), an association that is considered to continue throughout the disease course (Abner *et al.*, 2011). Furthermore, the inhibition of abnormal tau hyperphosphorylation and its aggregation appear to be promising therapeutic strategies in Alzheimer's disease. Thus, non-invasive imaging of tau pathology would be useful to assist in the early and differential diagnosis of dementia, track the progression of disease-related pathology, and monitor the efficacy of anti-tau treatments.

^{18}F-FDDNP has been reported to detect neurofibrillary tangle deposition (Shoghi-Jadid *et al.*, 2002) and successfully differentiate subjects with Alzheimer's disease and mild cognitive impairment from those with no cognitive impairment (Small *et al.*, 2006). However, this tracer detects the combined signals of senile plaques and neurofibrillary tangles (Shoghi-Jadid *et al.*, 2002). Several radiotracers have been developed for the selective visualization of neurofibrillary tangles in the living brain (Chien *et al.*, 2013, 2014; Maruyama *et al.*, 2013). Early clinical PET studies successfully differentiated patients with Alzheimer's disease from cognitively normal elderly. However, the selective binding ability of these radiotracers to tau has not been fully validated *in vivo*.

For the development of a selective tau radiotracer, we screened β-sheet-binding small molecules and identified novel quinoline derivatives with high binding selectivity to tau deposits in Alzheimer's disease brain samples (Okamura *et al.*, 2005; Fodero-Tavoletti *et al.*, 2011; Harada *et al.*, 2013). Through a compound optimization process, we developed a novel ^{18}F-labelled 2-arylquinoline derivative, ^{18}F-THK5105 (Fig. 1), which showed high binding affinity and selectivity to tau protein deposits in Alzheimer's disease brain sections (Okamura *et al.*, 2013). This ^{18}F-labelled radiotracer also exhibited high blood–brain barrier permeability and no defluorination in mice (Okamura *et al.*, 2013). The present clinical study evaluated whether ^{18}F-THK5105 PET could selectively bind to tau pathology in living patients with Alzheimer's disease.

Materials and methods

Participants

Sixteen subjects, including eight patients with probable Alzheimer's disease (three male and five females, age range 66–82 years) and eight age-matched healthy control subjects (three male and five females, age range 63–76 years), underwent both ^{18}F-THK5105 and ^{11}C-labelled Pittsburgh compound B (^{11}C-PiB) PET scans (Table 1). Written informed consent was obtained from all participants. Study approval was obtained from the Austin Health Human Research Ethics Committee. Elderly healthy controls were recruited by advertisements in the community, and patients with Alzheimer's disease were recruited from tertiary Memory Disorders Clinics or physicians who sub-specialize in dementia care. All participants were reviewed and classified on the basis of their clinical and neuropsychological performance by the consensus of a neurologist and a neuropsychologist who were blind to their PET results. The diagnosis of Alzheimer's disease was made according to the National Institute of Neurological and Communicative Disorders and Stroke/Alzheimer's Disease and Related Disorders Association (NINCDS-ADRDA) criteria.

Neuropsychological evaluation

Cognitive impairment and dementia severity were evaluated with the Mini-Mental State Examination (MMSE), the Clinical Dementia Rating (CDR) and the CDR scale sum of boxes (CDR-SOB). In addition, composite episodic memory and non-memory scores were generated as previously described (Villemagne *et al.*, 2011). Briefly, a composite episodic memory score was calculated by taking the average of the z-scores for the Rey Complex Figure Test, the long delay California Verbal Learning Test, Second Edition, and the Logical Memory II subscale of the Wechsler Memory Scale. A composite non-memory score was calculated by taking the average of the z-scores for the Boston Naming Test, letter fluency, category fluency, digit span forwards and backwards, digit symbol-coding, and Rey Complex Figure Test copy.

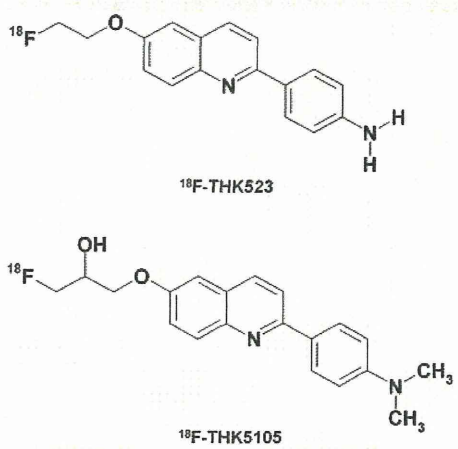

Figure 1 Chemical structures of ^{18}F-THK523 and ^{18}F-THK5105.

Table 1 Demographic characteristics of healthy control and Alzheimer's disease subjects

	Healthy controls (n = 8)	Alzheimer's disease (n = 8)
Age	70.5 ± 4.4	74.1 ± 6.9
Gender (M/F)	3/5	3/5
Years of education	15.4 ± 2.4	11.3 ± 3.2*
CDR	0.0	0.9 ± 0.5*
CDR-SOB	0.0	6.1 ± 4.9*
MMSE score	28.8 ± 1.5	17.3 ± 6.6*
Episodic memory scores	−0.1 ± 0.8	−3.8 ± 0.3*
Non-memory scores	−0.1 ± 0.5	−3.0 ± 1.9*
Grey matter volume (cm^3)	302.7 ± 12.9	272.9 ± 22.6*
Hippocampal volume (cm^3)	4.8 ± 0.5	4.0 ± 0.6*

*P < 0.05 by the Mann–Whitney U test.

Image acquisition

MRI scanning was performed on a 3 T Siemens TRIO magnetic resonance system (Siemens Healthcare) using the ADNI 3D MPRAGE sequence with 1 × 1 mm in-plane resolution and 1.2 mm slice thickness, repetition time/echo time/inversion time = 2300/2.98/900, flip angle 9°, field of view 240 × 256, and 160 slices. T_2 fast spin echo and FLAIR sequences were also obtained.

Two radiotracers, ^{18}F-THK5105 and ^{11}C-PiB, were prepared in the Centre for PET at Austin Hospital. ^{18}F-THK5105 was synthesized by *nucleophilic substitution of the tosylate precursor as described previously* (Okamura *et al.*, 2013). The decay-corrected average radiochemical yield of the production of ^{18}F-THK5105 was 45%, with a radiochemical purity >95% and a specific activity of 229.6 GBq/μmol (6.2 ± 3.3 Ci/μmol). ^{11}C-PiB was synthesized using the one-step *^{11}C-methyl triflate approach as previously described* (Rowe *et al.*, 2007). The decay-corrected average radiochemical yield for ^{11}C-PiB was 30%, with a radiochemical purity >98% and a specific activity of 30 ± 7.5 GBq/μmol.

A list-mode emission acquisition on an Allegro™ PET camera (Philips Medical Systems) was performed in 3D mode from 0–50 min and between 90–120 min after injection of 200 MBq ^{18}F-THK5105. List-mode raw data for the initial 50 min of the acquisition were sorted off-line into 6 × 30-s, 7 × 1-min, 4 × 2.5-min, 2 × 5-min, and 6 × 10-min frames. The final 30 min were acquired as 6 × 5-min frames. The sorted sinograms were reconstructed using a 3D RAMLA algorithm. A 30-min acquisition (6 × 5-min frames) on an Allegro™ PET camera began 40 min after intravenous injection of 300 MBq ^{11}C-PiB.

Image analysis

Hippocampal and cortical grey matter volumes were obtained using an automated volumetric measurement program (NeuroQuant: CorTechs Labs Inc) applied to the 3D MP RAGE MRI images. The primary MRI outcome measures were the grey cortical matter and hippocampal volumes normalized to total intracranial volume.

PET images were processed using a semi-automatic region of interest method. Firstly, standardized uptake value (SUV) images of ^{18}F-THK5105 and ^{11}C-PiB were obtained by normalizing tissue radioactivity concentration by injected dose and body weight. Subsequently, individual MRI T_1 images were anatomically co-registered into individual PET images using Statistical Parametric Mapping software (SPM8: Wellcome Trust Centre for Neuroimaging, London, UK). Co-registered MRI and PET images were then spatially normalized to an MRI T_1 template in Talairach space using SPM8. After spatial normalization, a region of interest template was placed on individual axial images in the cerebellar hemisphere, ventrolateral frontal cortex [Brodmann areas (BA) 10, 44, 45 and 46], lateral and medial orbitofrontal cortex (BA 11 and 12), superior temporal cortex (BA 22), inferior temporal cortex (BA 20 and 37), parietal cortex (BA 39 and 40), lateral occipital cortex (BA 18 and 19), anterior cingulate cortex, *posterior cingulate cortex, mesial temporal cortex* (BA 27, 28, 34 and 35), putamen, pons, and subcortical white matter. Regional SUVs were sampled using PMOD software (PMOD Technologies, Ltd).The ratio of regional SUV to cerebellar cortex SUV ratio (SUVR) was used as an index of tracer retention. Neocortical tau and amyloid-β burden were *expressed as the average SUVR for the following cortical regions of* interest: frontal, parietal, lateral temporal, and posterior cingulate for THK5105 and PiB, respectively. As in previous studies, a PiB SUVR threshold of 1.5 was used to categorize high and low amyloid-β burden.

Statistical analysis

Mann-Whitney's U-tests were applied for comparison of the Alzheimer's disease and healthy control groups. For comparison of regional radiotracer uptake, one-way repeated measures analysis of variance (ANOVA) followed by Bonferroni's tests were performed. To examine the regional difference of tracer retention between neocortex and mesial temporal cortex, Wilcoxon matched-pairs signed rank tests were performed. Effect size coefficients (Cohen's d) were calculated for the evaluation of group differences in PET measurements. Statistical significance for each analysis was defined as $P < 0.05$. Data are presented as mean ± standard deviation (SD).

Results

Healthy control and Alzheimer's disease subject demographics are shown in Table 1. There were no significant differences between healthy control and Alzheimer's disease groups with regard to age